Particle-based modelling of oxygen discharges

Franz X. Bronold[1], Konstantin Matyash[2], David Tskhakaya[3], Ralf Schneider[2], and Holger Fehske[1]

[1] Institut für Physik, Universität Greifswald, D-17489 Greifswald, [2] Max-Planck-Institut für Plasmaphysik, Teilinstitut Greifswald, D-17491 Greifswald, [3] Institut für Theoretische Physik, Universität Innsbruck, A-6020 Innsbruck, Österreich

Abstract

We present an one-dimensional particle-in-cell Monte-Carlo model for capacitively coupled radio-frequency discharges in oxygen. The model quantitatively describes the central part of the discharge. For a given voltage and pressure, it self-consistently determines the electric potential and the distribution functions for electrons, negatively charged atomic oxygen, and positively charged molecular oxygen. Previously used collision cross sections are critically assessed and in some cases modified. Provided associative detachment due to metastable oxygen molecules is included in the model, the electro-negativities in the center of the discharge are in excellent agreement with experiments. Due to lack of empirical data for the cross section of this process, we propose a simple model and discuss its limitations.

Motivation [1]

Oxygen discharges are particularly interesting because of the weak electro-negativity of O_2 and the presence of meta-stable O_2 states which lead to a competition between ion-ion neutralization and detachment due to neutrals. We focus here on capacitively coupled radio-frequency discharges in O_2.

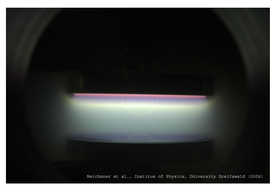

Fig. 1: Capacitively coupled radio-frequency discharge of oxygen (K. Dittmann et al. [1]). The parameters are: $L = 2.5 - 4\ cm$, $p = 10 - 60\ Pa$, $U_{rf} \sim 100 - 800\ V$, and $f_{rf} = 13.6\ MHz$.

The occurrence of negative ions (here O^-) leads to abrupt changes in the ion density which in most cases forces the discharge to stratify into a quasi-neutral ion-ion and a peripheral electro-positive edge plasma. Because of the spatial inhomogeneity, O_2 discharges are computationally challenging.

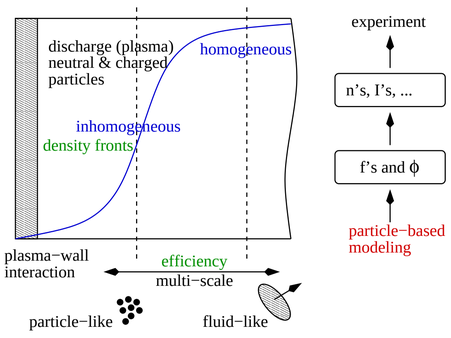

Method of simulation [2]

The description of an oxygen discharge could be based on a brute force numerical solution of the Boltzmann-Poisson system which couples the distribution functions of the relevant species with the electric potential.

$$\left[\partial_t + \mathbf{v}_i \cdot \nabla_r - \left(\frac{q}{m}\right)_i \nabla_r \Phi \cdot \nabla_v\right] f_i = I[\{f_j\}] \quad (1)$$

$$\Delta_r \Phi = -\frac{1}{\epsilon_0} \sum_{i,\mathbf{v}} q_i f_i \quad (2)$$

In most cases, however, this approach is not practical, even when, as we do, only e, O^-, and O_2^+ are the "kinetic species". More promising are methods which track the spatio-temporal evolution of a sample of particles subject to elastic, inelastic, and reactive collisions (PIC-MCC). These approaches are based on a decoupling of the free flights (in the self-consistent electric field) from the collisions. Thus, they are one-to-one representations of the statistical microphysics underlying the Boltzmann-Poisson system.

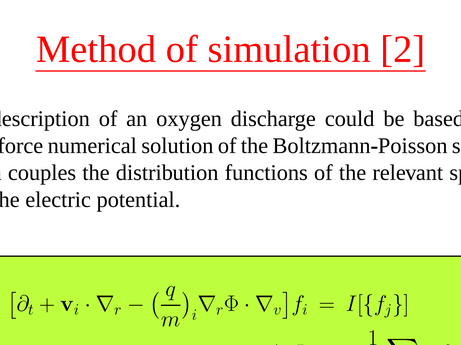

Model for an O_2 discharge [3]

Our simulations are restrict to the central axial part of the discharge. Ignoring the (electric) asymmetry between the grounded and powered electrode, we use an one-dimensional (1D) model, which keeps only one spatial coordinate but retains all three velocity coordinates.

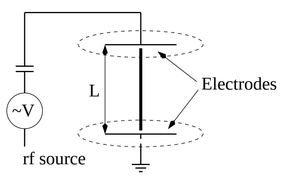

Fig. 2: Schematic geometry of the planar, 1D model on which the simulation is based. The boundary conditions are $\Phi = 0$ at $x = 0$, $\Phi = U_{rf}(t)$ at $x = L$, and absorbing electrodes for the particles.

The complex plasma-chemistry of oxygen gives rise to a large number of non-reactive and reactive collisions. In the table below we show the collisions included in our model. We simulate only e, O^-, and O_2^+ (three species plasma model). Neutral particles appearing either as reactants or products are not simulated: O_2 is modelled as a reservoir and O, $O_2(\nu)$, $O_2(\mathrm{Ryd})$, $O_2(a^1\Delta_g)$, and $O_2(a^1\Sigma_g)$ are only accounted for in as far as their production results in an energy loss for electrons.

The meta-stable $O_2(a^1\Delta_g)$ requires special attention because it also appears in the entrance channel for associative detachment (20). Its concentration is therefore important, and we should actually build-up the $O_2(a^1\Delta_g)$ distribution function, that is, we should also simulate $O_2(a^1\Delta_g)$ particles. In that case, however, not only their production process (14) but also their loss processes should be included. In addition, since $O_2(a^1\Delta_g)$ preferentially decays on the surface, a full description of the $O_2(a^1\Delta_g)$-wall interaction would be also required. This is beyond the 1D model. To take associative detachment, which is known to be an important process, nevertheless into account, we use instead a simple model with one free parameter, which can be interpreted as the $O_2(a^1\Delta_g)$ to O_2 density ratio (see below).

Table 1: Elastic, inelastic, and reactive collisions included in our model.

elastic scattering	
(1) $e + e \rightarrow e + e$	
(2) $O^- + O^- \rightarrow O^- + O^-$	
(3) $O_2^+ + O_2^+ \rightarrow O_2^+ + O_2^+$	
(4) $e + O_2^+ \rightarrow e + O_2^+$	
(5) $e + O^- \rightarrow e + O^-$	
(6) $O^- + O_2^+ \rightarrow O^- + O_2^+$	
(7) $e + O_2 \rightarrow e + O_2$	
(8) $O^- + O_2 \rightarrow O^- + O_2$	
(9) $O_2^+ + O_2 \rightarrow O_2 + O_2^+$	
electron energy loss scattering	
(10) $e + O_2 \rightarrow e + O_2(\nu = 1, ..., 4)$	
(11) $e + O_2 \rightarrow e + O_2(\mathrm{Ryd})$	
(12) $e + O_2 \rightarrow e + O(3P) + O(3P)$	(6.4 eV)
(13) $e + O_2 \rightarrow e + O(3P) + O(1D)$	(8.6 eV)
(14) $e + O_2 \rightarrow e + O_2(a^1\Delta_g)$	
(15) $e + O_2 \rightarrow e + O_2(b^1\Sigma_g)$	
electron & ion production & loss	
(16) $e + O_2^+ \rightarrow O + O$	
(17) $O^- + O_2^+ \rightarrow O + O_2$	
(18) $e + O_2 \rightarrow O + O^-$	
(19) $O^- + O_2 \rightarrow O + O_2 + e$	
(20) $O^- + O_2(a^1\Delta_g) \rightarrow O_3 + e$	
(21) $e + O_2 \rightarrow 2e + O_2^+$	
(22) $e + O^- \rightarrow O + 2e$	

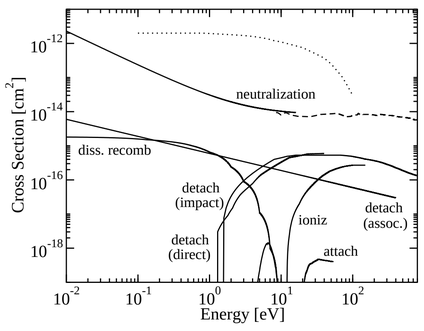

Fig. 3: Cross sections for dissociative recombination, neutralization, dissociative attachment, direct detachment, associative detachment, impact ionization, and impact detachment. The dashed line indicates the experimentally determined high-energy asymptotic of the neutralization cross section and the dotted line is the cross section for neutralization used in [8].

Our collection of cross sections is semi-empirical, combining measured data with simple models for the low-energy asymptotic, which is usually not very well known from experiments. In general, the high-energy asymptotic has to be also determined from models, but is less critical because the distribution functions decay sufficiently fast at high energies. We extrapolated therefore the values of the cross sections for the largest energies shown in the plots to all energies above it. Some of the cross sections significantly deviate from the ones previously used [8]. Our results indicate, however, that the modifications are essential for obtaining central electro-negativities in accordance with experiments [1, 7]. Two examples suffice to make the point:

Ion-Ion neutralization

For ion-ion neutralization (17), we constructed a cross section from a simple two-channel Landau-Zener model [4], with one free parameter, which we adjusted to obtain the correct high-energy asymptotic of the cross section [5].

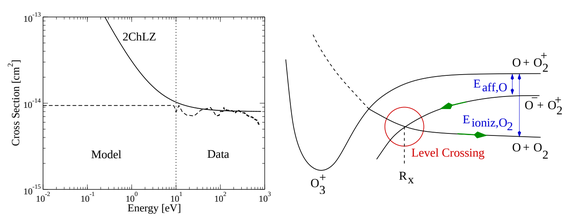

Fig. 4: Cross section for neutralization and the energetics of the corresponding Landau-Zener model.

$$\sigma_n(E) \approx 0.8\left(1 + \frac{2.85}{E[eV]}\right) \cdot 10^{-14} cm^2 \quad (3)$$

Detachment on neutrals

There is no evidence for associative detachment (20) in beam experiments [6]. Yet, investigations of O_2 discharges strongly suggest that this process is possible because of the meta-stable $O_2(a^1\Delta_g)$ [7]. We could not find an empirical cross section for associative detachment due to $O_2(a^1\Delta_g)$, we employed therefore a simple model, which describes the detachment as the "inverse" of a Langevin-type electron capture into an attractive auto-detaching state of O_3^-.

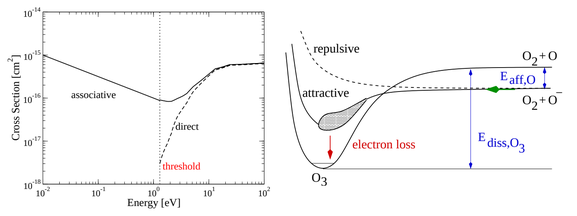

Fig. 5: Cross section for associative and direct detachment and the energetics of the "inverse" Langevin-type electron capture model.

$$\sigma_{ad}(E) \approx 5.96 \cdot \frac{10^{-16} \cdot cm^2}{\sqrt{E[eV]}} \quad (4)$$

From the cross section alone we cannot determine the probability P_{ad} for associative detachment. We also need the density of $O_2(a^1\Delta_g)$, which is unknown in the three species plasma model. However, it should be of the order of the O_2 density. Therefore, we write $n_\Delta = C \cdot n_{O_2}$, with $C < 1$, and obtain

$$P_{ad} = u \cdot \sigma_{ad} \cdot (C \cdot n_{O_2}) \cdot t_{c,1}, \quad (5)$$

where C is a fit parameter which can be adjusted to experiments.

Results [3, 9]

Direct vs. associative detachment

To determine C, we simulated the discharge described by Katsch [7] for $p = 13.8\ Pa$, $U_{rf} = 250\ V$, and $f_{rf} = 13.6\ MHz$, and tuned C to reproduce the central axial negative and positive ion densities at $x = L/2$ (central densities); the central electron densities match then also because of quasi-neutrality in the bulk of the discharge. We obtained $C \approx 1/6$, implying that roughly one sixth of the O_2 molecules is in the meta-stable state.

In Fig. 6 we plot the central ion and electron densities for $p = 13.8\ Pa$ over a wide voltage range, using for all voltages $C \approx 1/6$, the value determined for $U_{rf} = 250\ V$. The agreement between simulation and experimental data [7] is rather good, with simulated densities deviating from the measured ones by less than 10%, indicating that our model captures the essential processes in the bulk of an oxygen discharge.

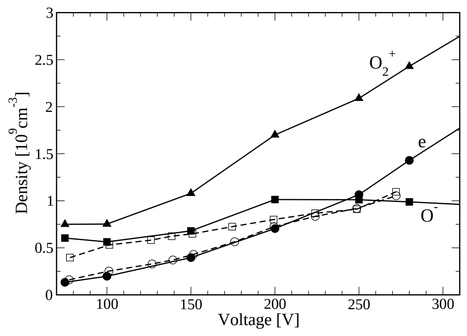

Fig. 6: Voltage dependence of the central electron and ion densities for a discharge with $L = 2.5\ cm$, $p = 13.8\ Pa$, and $f_{rf} = 13.6\ MHz$. Filled (open) symbols denote results of the simulation (measured densities [7]). Solid and dashed lines guide the eye.

Associative detachment (20) is the critical process for the correct modelling of the experiment. Without it, we could not even obtain the correct order of magnitude for the central densities. It is also remarkable that without associative detachment, the density profiles are very parabolic, as expected from ambipolar drift-diffusion models.

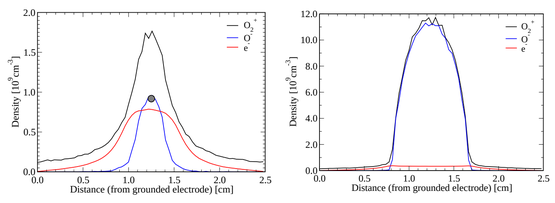

Fig. 7: The left (right) panel shows the electron and ion density profiles for $U_{rf} = 250\ V$ with (without) associative detachment taken into account. Experimentally, $n_e \approx n_{O^-} \approx 0.9 \cdot 10^9\ cm^{-3}$ (grey bullet) [7]. p, L, and f_{rf} are the same as in Fig. 6.

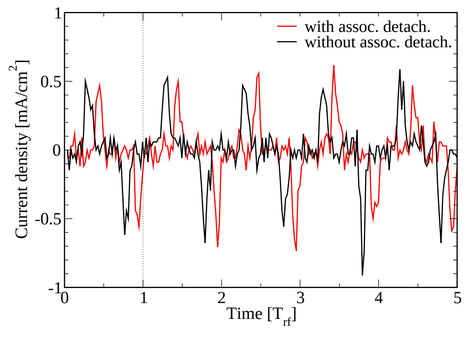

Fig. 8: Time dependence (for five rf cycles with duration T_{rf}) of the current densities corresponding to the cycle-averaged, quasi-stationary density profiles shown in Fig. 7.

Whereas the simulation with associative detachment reproduces reasonably well the densities of charged particles in the center of the discharge, the shapes of the (axial) density profiles deviate from the measured ones. Compared to experiment, the central plasma is too narrow, most notably, for lower voltages (not shown here) [3]. This is a shortcoming of the three species plasma model which ignores the spatial dependence of the $O_2(a^1\Delta_g)$ density which, in reality, results from the interplay of volume and surface loss and generation processes. Because the probability of associative detachment is proportional to n_Δ, the $O_2(a^1\Delta_g)$ density profile should strongly affect the density profiles of charged particles.

Note, the current densities are almost the same, irrespective of whether associatvie detachment is taken into account or not. This could imply that two rather different density profiles may be consistent with a given external power supply. Which configuration is realized depends then on the outcome of the competition between ion-ion neutralization and associative detachment.

844 nm emission

We also used our model to find a microscopic explanation for the experimentally observed spatial profile of the $844\ nm$ emission in front of the powered electrode of a rf discharge in O_2 [1].

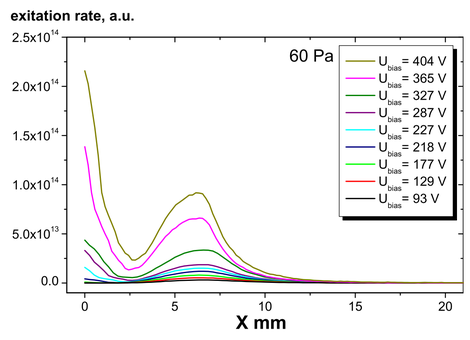

Fig. 9: Simulated $844\ nm$ emission intensity for $p = 60\ Pa$ and various U_{rf} as a function of the distance from the powered electrode. For a comparison with experiment see [9] and Poster 429 by K. Dittmann and coworkers.

Since the microscopic origin of this emission is a transition of the atomic oxygen ($O^*(3p^5P) \rightarrow O(3s^5S)$), we assumed electron-molecule and ion-molecule dissociative excitation of the O_2 molecule to be responsible, respectively, for the peak at $x \neq 0$ and the increase for $x \rightarrow 0$. Writing

$$I_{844nm}(x) \sim \langle \sigma^e_{de} \cdot u \cdot f_e \rangle_{rf} + \langle \sigma^i_{de} \cdot u \cdot f_i \rangle_{rf} \quad (6)$$

and using $\sigma^i_{de}(E) = \sigma^i_0 \theta(E - E^i)$, with σ^i_0 and E^i two fit-parameters, which we fixed for $U = 100\ V$, we found excellent agreement over a large range of voltages [9].

Support for our interpretation comes from phase-sensitive measurements and simulations, which clearly show that the peak at $x \neq 0$ is modulated by f_{rf}, and is thus of electronic origin, and the fact that close to the electrode the only heavy ions with a non-negligible density, and thus a sizeable scattering probability, are the O_2^+.

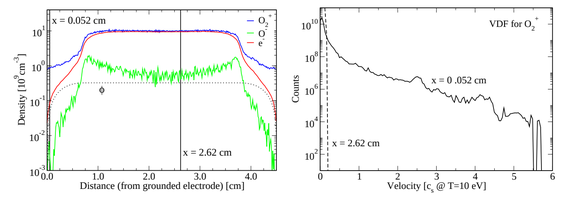

Fig. 10: Simulated electron and ion density profiles for the EMAU experiment [1]: $p = 60\ Pa$ and $U_{rf} = 800V$.

Conclusion and outlook

We presented a planar, 1D, three-species PIC-MCC model (e, O^-, and O_2^+) for a capacitively coupled rf discharge in O_2, capable to quantitatively describe experiments. Neutral particles are only indirectly incorporated via collisions with the simulated charged particles. This is sufficient to reproduce central electron and ion densities. However, the (axial) ion density profiles of the simulation are too narrow compared to the experimental ones. We expect better agreement when the $O_2(a^1\Delta_g)$ density profiles are also obtained from a kinetic model. Work in this direction is in progress.

Support from the SFB-TR 24 "Complex Plasmas" is greatly acknowledged. We thank B. Bruhn, H. Deutsch, K. Dittmann, and J. Meichsner for discussions and K. Matyash and R. Schneider acknowledge funding of the work by the Initiative and Networking Fund of the Helmholtz Association.

References

[1] K. Dittmann *et al.*, submitted.

[2] K. Matyash, *Kinetic modelling of multi-component edge plasmas* (PhD thesis, Universität Greifswald, 2003).

[3] F. X. Bronold *et al.*, submitted; arXiv:0705.0495v1.

[4] R. E. Olson, J. Chem. Phys. **56**, 2979 (1972).

[5] R. Padgett and B. Peart, J. Phys. B **31**, L995 (1998).

[6] J. Comer and G. J. Schulz, J. Phys. B **7**, L249 (1974).

[7] H. M. Katsch *et al.*, Plasma Source Sci. Technol.**9**, 323 (2000).

[8] V. Vahedi and M. Surendra, Comput. Phys. Commun. **87**, 179, (1995).

[9] K. Matyash *et al.*, submitted.